

**REVIEW OF AERONAUTICAL FATIGUE
INVESTIGATION IN JAPAN
DURING THE PERIOD JUNE 2001 TO MAY 2003**

Edited by

**Akira Kobayashi
The University of Tokyo**

and

**Hiroyuki Terada
National Aerospace Laboratory**

**For Presentation at the 28th Conference of
the International Committee on Aeronautical Fatigue**

Lucerne, Switzerland, May 6, 2003

| CONTENTS | Page |
|--|-------------|
| 12.1 INTRODUCTION | 12/3 |
| 12.2 LIFE EVALUATION ANALYSIS | 12/4 |
| 12.2.1 Development of Hybrid Bayesian Analysis Code for Continuing Integrity of Aircraft Structures | 12/4 |
| 12.2.2 Reliability-Based Calendric Inspection Schedule for Aircraft Structures with Corrosion Fatigue | 12/4 |
| 12.2.3 A Probabilistic Approach to Predicting Fatigue Life of Corroded Airframe Material | 12/5 |
| 12.3 METALS | 12/6 |
| 12.3.1 Fatigue Properties of a Stainless Steel Strip for an Erosion Cap of Helicopter Rotor Blades in a Large Strain Region | 12/6 |
| 12.3.2 D357 Casting Door Development Test | 12/7 |
| 12.4 COMPOSITES | 12/8 |
| 12.4.1 Real-time Detection of Edge Delamination in Composite Laminates under Fatigue Loading Using Embedded Small-Diameter Fiber Bragg Grating (FBG) Sensors | 12/8 |
| 12.4.2 Composite Fuselage Demonstrator for Damage Detection and Suppression Using Smart Health Monitoring System | 12/9 |
| 12.4.3 Fatigue Properties of CFRP laminates with embedded pre-strained SMA foils | 12/11 |
| 12.4.4 Full Scale Component Tests of Composite Wing Control Surfaces - EMBRAER170 | 12/12 |
| 12.5 FULL-SCALE TESTING | 12/13 |
| 12.5.1 Strength Tests for Japanese New Military Aircraft | 12/13 |
| 12.6 AIRCRAFT ACCIDENT INVESTIGATION | 12/15 |
| 12.6.1 Aircraft Accident Investigation in Japan | 12/15 |
| 12.7 ICAF DOUCUMENTS DISTRIBUTED BY JAPAN DURING 2001 ~2003 | 12/16 |
| ACKNOWLEDGMENTS | 12/16 |
| TABLES AND FIGURES | 12/17 |
| (Last page | 12/30) |

12.1 INTRODUCTION

A. Kobayashi, National Delegate, e-mail: ogihara@rs.noda.tus.ac.jp

The present national review reports aeronautical fatigue activities in Japan during 2001 to 2003. The very review is due to contributions by Aeronautical Fatigue Research Committee members of Japan Society for Aeronautical and Space Sciences, especially to the key members affiliated with the following:

National Aerospace Laboratory (NAL)

Third Research Center, Technical Research and Development Institute (TRID), Japan Defense Agency (JDA)

Aircraft and Railway Accident Investigation Commission (ARAIC)

Mitsubishi Heavy Industries, Ltd. (MHI)

Kawasaki Heavy Industries, Ltd. (KHI)

Fuji Heavy Industries, Ltd. (FHI)

University of Tokyo

Tokyo Metropolitan Institute of Technology

The above-mentioned members are greatly appreciated for their concentrated endeavor to achieve such a fruitful review.

Mr. Tadao Kamiyama, the first and former National Delegate of Japan, is acknowledged for his everlasting encouragement during the course of compilation of the present review.

12.2 LIFE EVALUATION ANALYSIS

12.2.1 Development of Hybrid Bayesian Analysis Code for Continuing Integrity of Aircraft Structures

S. Ito, and W. Bintuan, National Aerospace Laboratory of Japan (NAL), e-mail : itoh@nal.go.jp

In the aircraft structure in which the damage tolerance design has been introduced, the structural inspection and the repair or replacement of damaged structural elements detected in the inspection play a very important role for maintaining desirable safety of aircraft structure. In order to obtain an adequate inspection schedule for the structures, many of uncertain parameters concerning structural damage in the elements, such as strength degradation caused by damages, element failure, and detectability of damages should be evaluated. However, it is actually impossible to obtain sufficient data due to the restriction of cost affairs and the time dependency. Especially, information available prior to service is, in most cases, a most restricted one.

As an effective method to comply with the reliability analysis that can rationally estimate the characteristics of uncertain parameters of the structure is proposed to evaluate the structural integrity with the use of Bayesian theory and non-parametric estimation method based on ABIC(Akaike Bayesian Information Criteria). Past experience and engineering judgment are introduced as prior information before the structural operation in order to supplement such information shortage applying fuzzy theory and ABIC theories to the initial estimation process. In addition, the conventional Bayesian method to estimate uncertain parameters is also considered by the utilization of structural operation data obtained from the inspection results. Subjective information is often given by inspection results because of fuzzy environment which arises from the inspector's judgment. An attempt is also made to consider fuzzified Bayesian method in order to obtain posterior probability of parameters from the information.

The structure of hybrid Bayesian analysis code(HYBAC) for structural reliability evaluation is given in Figure 12.1. First the unknown parameters related to damage tolerance design are estimated from the information prior to service. The major steps of the model are parametric/non-parametric estimation based on Bayesian method, evaluation of structural reliability from the estimation results, and collection of the operational field data information for the next Bayesian evaluation. Numerical examples are presented to demonstrate the effectiveness of the HYBAC method on continuing aircraft structural integrity.

12.2.2 Reliability-based Calendric Inspection Schedule for Aircraft Structures with Corrosion Fatigue

S. Ito and W. Bintuan, National Aerospace Laboratory of Japan (NAL), e-mail : itoh@nal.go.jp

Corrosive environment is recognized as a significant factor that affects the reliability,

durability and integrity of aircraft. A quantitative approach for defining suitable inspection schedule and mandatory repairs is necessary for an effective management of an aging fleet of aircraft or new airframe structures to be served in corrosive environment. Because many uncertain parameters are involved in reliability analysis of structures and the fact that it is impossible to obtain sufficient actual structural operation data in the present state, authors have developed an approach for non-periodic inspection based on Bayesian method. However, the application of the present approach to structures with corrosion impact has not been attempted, and is the principal investigation of the paper. The analysis procedure is performed by two steps: failure process simulation with true structural element model (step I), and Bayesian analysis for inspection schedule of the entire structure model (step II). The influences of flight frequency and crack detection capability are also examined.

A typical commercial transport fuselage structure with fatigue critical elements is used as a realistic model for the present analysis. The model is shown in Figure 12.2. Each element comprises a skin panel and three frames and is subjected to pressurization-depressurization cycling. The structure is assumed to be exposed to aqueous corrosion environment as well as no-corrosion environment. Undetermined aspects considered are fatigue crack initiation and propagation, failure rate function and crack detection capability. Monte Carlo method is adopted to demonstrate the validity of the Bayesian reliability analysis. As a result, the optimum non-periodic calendric inspection schedule is implemented. Also, the uncertain parameters are estimated using the information gathered during the inspection. With the suggested procedure and parameter values, non-periodically inspection intervals for both cases of corrosion and no-corrosion are established. The implemented results are shown in Figure 12.3.

For case of corrosion, with the same detection capability the first inspection time and the intervals between the subsequent inspections are obviously shorter than that for case of no-corrosion. The structure with more frequent daily flight requires much shorter inspection intervals to sustain their reliability level. However, less inspection times is required with the aid of higher crack detection capacity. Due to earlier crack initiation and higher crack propagation rate for structural elements with corrosion, however, the requirements for damage detection and inspection should be more stringent. It should be mentioned in the numerical example, that the selection of parameter values for corrosion model is somewhat arbitrary that refers to insufficient data, but the analytical results remain qualitatively practical. In reality, aircraft structures (including rivet holes) are protected quite well; however, when they have been compromised by corrosion, corrective action such as repair becomes urgent.

12.2.3 A Probabilistic Approach to Predicting Fatigue Life of Corroded Airframe Material

Q.X. Yang, Northwestern Polytechnical University (NPU), W. Bintuan and S. Ito, National Aerospace Laboratory of Japan (NAL), e-mail : itoh@nal.go.jp

Corrosive environment and aging effect on aluminum alloys are recognized as significant degradation factors that affect the reliability, durability and integrity of aircraft structures. A practical approach is necessary for assessing the durability and integrity of structures. Prediction of fatigue reliability and calendric service time require statistically accurate estimates of materials fatigue response for loading and environment conditions. When the practical engineering approach-Miner's rule is used to calculate the fatigue damage, these estimates often involve the statistical characteristics of fatigue cumulative damage, especially those involving corrosion and aging effect of materials. To meet these needs, a phenomenological probability model is developed, which is based on the deterministic calendric fatigue life predicting approach and cumulative fatigue damage dynamic interference statistical model.

The model is developed similarly to the classical stress-strength interference reliability model. The cumulative fatigue damage is a time dependent random variable, which depends on the material properties and loading, but the critical cumulative damage is a random variable that should only depend on the material properties. However, the material properties may be degraded by the effect of the long-term corrosion and ageing. As an application example of typical enter-hole aluminum alloy specimens loaded by random spectrum loading, comparison between the predicted results and experimental distribution is shown in Figure 12.4. From the figure, it is shown that the proposed model can successfully predict the fatigue reliability of materials under constant amplitude and random loading spectrum. Because the model utilizes the time dependent cumulative fatigue damage interference statistical approach and modified Miner's rule, and particularly, considers the corrosion and ageing effects of materials and the variation in their fatigue statistical characteristics, it is reasonable and suitable for assessing the calendric fatigue life of an ageing fleet of aircraft and new airframe structures.

12.3 METALS

12.3.1 Fatigue Properties of a Stainless Steel Strip for an Erosion Cap of Helicopter Rotor Blades in a Large Strain Region

T. Shimokawa, Tokyo Metropolitan Institute of Technology (TMIT), Y. Hamaguchi and S. Machida; National Aerospace Laboratory of Japan (NAL); T. Ogawa, Aoyama Gakuin University (AGU) and H. Itabe, Honda R&D Co., e-mail: shimoka@tmit.ac.jp

One of the design requirements of helicopter rotor blades made of GFRPs (Glass Fiber Reinforced Plastics) is to protect their surfaces from erosion or abrasion produced by foreign objects such as rains, sands, small stones, hailstones and etc. To satisfy this requirement, a metal erosion cap is bonded on the leading edges of composite rotor blades. Titanium alloys, electro-formed nickels and stainless steels are widely used for the erosion cap. Among them stainless steels are less expensive for material itself and processing and desirable for the erosion cap of civil helicopter rotor blades.

However, the erosion cap is loaded very high-strain cycles due to high flexibility of a glass

fiber/epoxy composite material used for blade spars. FHI (Fuji Heavy Industries, Inc.) estimated that during a high-speed cruise-flight, the endurance loading cycle was composed of the maximum strain to be $4,200\mu$ -strain and the minimum strain $2,200\mu$ -strain. Moreover, $4,200\mu$ -strain is very close to the yield strain of stainless steels. Therefore, this strain cycle is very high for stainless steels. Moreover, the S - N data under this high-strain loading were not published.

The objective of the present study was to evaluate statistical fatigue properties of a thin sheet of ASTM 5517 stainless steel (AISI 301, 1/4 hard) selected as a candidate material for the erosion cap. Tensile fatigue tests were conducted up to 10^7 cycles on unnotched specimens under constant amplitude loading with stress ratios $R = S_{\min}/S_{\max} = 0$ and 0.3 in a high-strain region, where S_{\min} is the minimum stress and S_{\max} the maximum stress in constant stress amplitude. Figure 12.5 indicates the specimen shape. Figure 12.6 presents S - N relationships. Figure 12.7 compares the design strain range with the mean fatigue strength at 10^7 cycles for $R=0$ and 0.3 .

The major results obtained are as follows: (1) Fifteen S - N data in the inclined region of an S - N curve for $R=0$, where S is stress amplitude, provided the standard deviation of log-life $\sigma_L = 0.126$ and the standard deviation of fatigue strength $\sigma_S = 22.6$ MPa. (2) Twenty one S - N data, seven at each of three stress levels, in the horizontal region of the S - N curve were obtained. Thirteen among twenty one data were run out at $N=10^7$ cycles. Let denote fatigue strength at $N=10^7$ by S_H . This data provided the mean, standard deviation, and the coefficient of variation of S_H to be $\bar{S}_H = 333$ MPa, $\sigma_H = 12.4$ MPa, $\eta_H = 3.73\%$ respectively. (3) On the basis of the test results the present study substantiated that the material tested was suitable for erosion caps of glass fiber/epoxy helicopter rotor blades.

12.3.2 D357 Casting Door Development Test

T. Sakagawa, Mitsubishi Heavy Industries, Ltd. (MHI), e-mail : toru_sakagawa@mx.nasw.mhi.co.jp

Objective;

The application of casting technology is expected the reduction of manufacturing cost and weight. MHI studied to apply the casting technology to the emergency exit door of transport airplane.

Design and manufacturing;

The casting door for regional transport airplane was designed with following specification,

Material: D357-T6 (AMS-4241)

Min. thickness: .060" (1.5 mm)

| | | |
|------------------------|----------------|----------------------------------|
| Geometrical tolerance: | Generic area | $\pm .060'' (\pm 1.5\text{mm})$ |
| | Interface area | $\pm .030'' (\pm 0.75\text{mm})$ |
| | Thickness | $\pm .010'' (\pm 0.25\text{mm})$ |

| | |
|------------------------|----------------------|
| Design pressure level: | 12.84 psi (Ultimate) |
| | 6.21 psi (Fatigue) |

| | |
|----------------------|----------------------|
| Design service goal: | 80,000 flight cycles |
|----------------------|----------------------|

Figure 12.8 shows the assembly part of casting emergency exit door. The door structure consists of one piece roll formed skin and one piece casting frame and beam. The assembly of door consists of two parts; the upper door is of inward motion, and the lower door is rotated outside around bottom hinge line attached to fuselage. The size of the upper door is 36.2" height by 19.8" width and the lower door is 18.5" height by 19.8" width. FEM internal load analysis and both static and durability/damage tolerant analysis have been conducted.

Strength test;

Limit and ultimate static test, fail -safe test considering one pressure stop ftg. Failure condition and durability/damage tolerant test have been conducted. The damage tolerant test also have been considered the reparability of casting including mechanical and welding repair.

Good agreement was found between test results and analysis for the displacement and strain measurements. Also the static strength and durability/damage tolerant capability of casting emergency door were confirmed.

Figure 12.9 and Figure 12.10 show the test specimen and test set-up configuration.

Conclusion;

The casting emergency exit door design and manufacturing process were confirmed the reduction of manufacturing cost and weight to compare with traditional build-up structure. It was confirmed to meet the strength requirement including the repair scheme after reviewing the test and analysis results.

12.4 COMPOSITES

12.4.1 Real-time Detection of Edge Delamination in Composite Laminates under Fatigue Loading Using Embedded Small-Diameter Fiber Bragg Grating Sensors

N. Takeda, S. Takeda and Y. Okabe, The University of Tokyo,

e-mail : takeda@compmat.rcast.u-tokyo.ac.jp

Edge delaminations in composite laminates tend to occur under fatigue loading because interlaminar shear and/or normal stresses become high at the free edge. Development of the real-time monitoring technique is necessary for evaluation of the edge delamination. In the present research, the authors attempted to detect the edge delamination using small-diameter FBG sensors whose diameter is about 1/3 of normal FBG sensors. This small-diameter FBG sensor can be embedded within one composite prepreg ply easily, which causes almost no strength deterioration of composite laminates.

Fatigue tests were conducted for quasi-isotropic $[45/-45/0/90]_S$ laminates under tensile-tensile

cyclic loading that was applied to the specimen from 0 to 440 MPa. The dimensions of test specimen are $140 \times 30 \times 1.0 \text{ mm}^3$. The frequency of the loading cycle is 5 Hz. When the broadband light was launched into the FBG sensor embedded into the specimen, the narrowband light was reflected and separated from the incident light through a circulator. After the cyclic loading was stopped at the pre-determined numbers of cycles, the spectrum of the reflected light was measured with an optical spectrum analyzer at both loading of 220 MPa and unloading conditions. The edge delamination was observed by the soft X-ray photograph and the edge delamination length, L_{ed} , was defined as the length of delamination in the width direction as shown in Figure 12.11 (a). In order to detect the edge delamination that propagated at $0^\circ/90^\circ$ interface or inside of 90° ply of the laminate, the small-diameter FBG sensor was embedded into 90° ply in contact with $0^\circ/90^\circ$ interface as shown in Figure 12.11 (b). The gage section of the FBG sensor was set at 0 to 10 mm from the center of the specimen.

Figure 12.12 shows the measured reflection spectra at various delamination lengths. The intensity of spectrum is normalized by the intensity of the highest component. Before the cyclic load was applied to the specimen, the spectrum had one peak. Though the delamination length increased, the drastic change in the form of spectrum was not observed under unloading. On the other hand, the spectrum measured at loading of 220 MPa changed its form with an increase in delamination length. If the tip of the edge delamination reached the location of the FBG sensor, the spectrum was divided into two peaks. As the delamination length increased, the intensity of the longer wavelength peak increased relatively. From the results, the edge delamination can be detected under loading conditions.

For confirmation of the measured results, the reflection spectrum was simulated by theoretical analysis. Solving couple mode equations with transfer matrix method simulated the spectrum using the strain distributions of the FBG sensor, which was calculated by 3-D FEM analysis. The tendency of change in the experimental results was the same as that in the theoretical results. Hence it was found that the edge delamination could be evaluated quantitatively by monitoring of the reflection spectrum from the small-diameter FBG sensor.

12.4.2 Composite Fuselage Demonstrator for Damage Detection and Suppression Using Smart Health Monitoring System

N. Takeda, The University of Tokyo, N. Tajima, and T. Sakurai, R&D Institute for Metals and Composites for Future Industries (RIMCOF), e-mail : takeda@compmat.rcast.u-tokyo.ac.jp

The Japanese Smart Material and Structure System Project started in 1998 and has been developing several key sensor and actuator elements. The present project consists of four research groups such as structural health monitoring, smart manufacturing, active/adaptive structures, and actuator materials/devices. In order to integrate the developed sensor and actuator elements into a smart

structure system and show the validity of the system, two demonstrator programs was manufactured. Both demonstrators were CFRP stiffened cylindrical structures with 1.5m in diameter and 3m in length. A Damage Detection and Suppression function was to be demonstrated by the first one, and the second one demonstrated a suppression of vibration and acoustic noise generated in the composite cylindrical structure. Seven themes were selected and classified into the following categories as shown in Table 12.1. They were also divided into two Demonstrators groups respectively, that is; (1) Damage Detection and Suppression: Theme #1 through #6 and (2) Noise and Vibration Reduction: Theme #7.

Figure 12.13 shows the outline of the Damage Detection and Suppression Demonstrator. The Demonstrator was mounted to the test frame on the cantilever mode. The shear load (approx. 20 tons max) was applied to the free end of the test article as a bending load. Internal pressure (0.75atm maximum) was also applied to the test article. Various levels of impact loads (approx. 50 joules maximum) were applied to the upper panel. The test was performed in the order of load-unload test, static test, pressure test and impact test. In the load-unload test, the bending load was gradually increased in a quasi-static condition. Before and after each test, visual and ultra-sonic inspections were performed. The following tests were conducted in the demonstrator: (1) Real Time Detection of Impact Damage Using Optical Fiber Sensors Embedded into CFRP Laminated Structures: using small-diameter optical fiber sensors embedded in the upper panel, detection of any impact damage and identification of its location were demonstrated. (2) Real Time Detection of Impact Damage Using Integrated Acoustic Emission Sensor Network Systems: using the AE sensors mounted on the side panel, time of occurrence, location and magnitude of the impact load were identified. (3) Strain Distribution Measurement in Wide Area Using Distributed BOTDR Sensors: using optical fibers embedded in the side panels and externally installed to the overall test article, damage location and its magnitude were identified from the measured strain distribution. (4) Damage Detection by Electric Conductivity Change in Smart Patch (Carbon fiber composite laminate): two types of smart patches, carbon fiber fracture type and laminate edge-delamination type were applied at the bottom panel of the demonstrator in load-unload test phase to demonstrate the smart patches to memorize the applied maximum strain and to measure the number of loading cycles, respectively. (5) Damage Suppression Using Embedded SMA (Shape Memory Alloy) Foils: it was verified that the shape memory alloy foils embedded in the bottom panel could suppress the occurrence and growth of damages. In the load-unload test phase, the evaluation was performed with CFRP laminates with and without embedded SMA foils. (6) Verification of Smart Manufacturing of Low Cost Integrated Panel by RTM (Resin Transfer Molding): an optical fiber sensor, used for monitoring the manufacturing on the bulkhead panel with RTM process, was verified in order to measure strains in the pressure test phase. A dielectric flow sensor was also used to monitor the resin flow front during the RTM process.

12.4.3 Fatigue Properties of CFRP Laminates with Embedded Pre-strained SMA Foils

T. Ogisu, M. Shimanuki and S Kiyoshima, Fuji Heavy Industries LTD.(FHI),
e-mail : ogisut@uae.subaru-fhi.co.jp

FHI developed new smart materials and structural systems for the application to the aircraft structure. The evaluation of the systems conducted both quasi-static load-unload and fatigue tests using some kinds of quasi-isotropic CFRP laminates with embedded SMA foils in recent study. It was found that the damage suppression effects were obtained by the suppression of the strain energy release rate based on the suppression of the crack opening displacement due to the recovery stress of SMA foils through the detailed observation of the damage behavior. (See Figure 12.14)

The coupon test specimens are 250mm in length, 35mm in width and 1.6mm in nominal thickness for CFRP only and 1.89 mm in nominal thickness for CFRP with embedded SMA. The gage length is 50mm. Table 12.2 shows the stacking sequence and test temperature of these test specimens.

Quasi-static load-unload tests were conducted at a constant cross-head speed (1mm/min) at both R.T. and 80°C. The test specimens were loaded until the predetermined strain levels of every 0.05% pitch from 0.2% to 1.2% at total applied strain. After that, the specimens were unloaded at the same cross-head speed until no load. Such loaded-unloaded cycles were repeated up to the final failure of test specimens. Figure 12.15 shows a set up situation of the test specimen. Transverse crack density was measured by irradiation of black light after immersing a penetrant solution at free edges of test specimens after each load-unload cycle. The transverse crack density was defined as the number of cracks divided by the gage length (5cm).

Table 12.3 shows the damage onset strain and Figure 12.16 shows the transverse crack density as a function of applied strain in load-unload tests. At specimens of No.1 and 2 types, the first transverse cracks generated at 0.67% strain at R.T. and 0.65% strain at 80°C. The number of transverse cracks increased as the applied strain increased. The crack density was larger for No.2 (tested at 80°C) than No.1(tested at RT). On the other hand, the transverse crack of CFRP laminates with embedded 2% pre-strained SMA was generated at 0.84% strain at R.T.(No.5) and 0.89% strain at 80°C (No.6). The increase rate of the transverse crack density at both RT and 80°C was almost the same. Then, in case of specimens of No.3 and 4 types, the onset of the transverse crack occurred at 0.7% strain at R.T.(No.3) and 0.75% strain at 80°C (No.4). Therefore, the smart CFRP laminates with embedded pre-strained SMA foils were increased by 0.22% on transverse crack onset strain as compared with conventional CFRP laminates. The improvement effect consist of the increase of 0.03% by embedded SMA foils, the increase of 0.15% by recovery stress at RT and the increase of 0.05% by the recovery stress caused by heating of 2% pre-strained SMA. As the test results, it was

confirmed that the onset strain of the transverse crack of CFRP laminates with embedded SMA foils increased 30% at R.T. and 35% at 80°C in comparison for the conventional CFRP laminates.

High cycle fatigue tests were conducted at RT and 80°C using both standard CFRP laminates (No.1 and 2) and CFRP laminates with embedded 2% pre-strained SMA foils (No.5 and 6) for determining the onset cycles of transverse crack and delamination. Figures 12.17 and 12.18 show the results of fatigue tests. Both onset cycles of transverse crack and delamination increased in the order of No.2 (CFRP, 80°C), No.1 (CFRP, RT), No.6 (CFRP with 2% pre-strained SMA, 80°C) and No.5 (CFRP with 2% pre-strained SMA, RT). For example, the onset cycle of transverse cracks was $N=300$ (No.2), $N=2000$ (No.1), $N=8000$ (No.6), and $N=50000$ (No.5) at 0.5% applied strain, respectively. It was expected that the specimen of No.6 type would show the most effective suppression effect for the damage onset strain. However, the maximum effect was obtained for the specimen of No.5 type. These phenomena are supposed that the recovery stress at 80°C is not sufficient to overcome the property reduction of 90° ply at 80°C. Furthermore, the CFRP with embedded 2% pre-strained SMA foils of both RT and 80°C obviously showed damage suppression effects at higher strain level over 0.5% strain. However, the difference of damage suppression effects between standard CFRP laminates and CFRP laminates with embedded pre-strained SMA became similar below 0.4% strain. Thus, the damage suppression effect caused by the both recovery stress and embedded effect of SMA was clearly observed at the higher strain level.

As mentioned above, the damage suppression effect of smart material using quasi-isotropic CFRP laminates with embedded SMA foils verified technically.

12.4.4 Full Scale Component Tests of Composite Wing Control Surfaces - EMBRAER170

K. Toyoda, K. Kosugi, H. Sashikuma and T. Taki, Kawasaki Heavy Industries, Ltd. (KHI)
e-mail : toyoda_k@khi.co.jp

Kawasaki Heavy Industries, Ltd. (KHI) is participating in the development of EMBRAER170 as a risk sharing partner and is developing most of wing structure except for skins and ribs of wing box. Six full scale component tests of wing control surfaces in parallel are under way from 2002 to 2003 at Gifu Works, KHI in Japan for type certification. The tests consist of four structural strength tests for inboard flap, outboard flap, aileron and spoiler, and two mechanism operation tests for inboard and outboard flap.

Figure 12.19 shows KHI's work share and component test items. Figure 12.20 shows the photographs of full scale component tests of wing control surfaces.

In the present paper, the structural strength test of inboard flap is presented as an example.

Structural strength test of inboard flap

The flap is a double slotted type and consists of main flap panel, aft flap panel and mechanism. The flap panels are mainly made of 180°C cure carbon/epoxy composites, KMS-6115. (KHI has developed KMS-6115, which is a new generation carbon/epoxy pre-preg for aircraft primary and secondary structures. This material was approved by JCAB and JAA, and FAA approval is underway.) The flap mechanism consists of two track supports with rails, two carriages and other parts.

The test fixture consists of a loading fixture (whiffletree), support fixture, environmental chamber and so on. The test loads are introduced to the lower surface of the flap panels with rubber pads in order to simulate the design load distribution. Three hydraulic actuators and whiffletrees are used to introduce static loads and fatigue load spectrum.

One test specimen (LH part) is used for the static and fatigue test. "No growth design concept" is applied to the flap composite structure for the damage tolerance substantiation. The static and fatigue strength of flap mechanism is also substantiated in the test.

The test procedure is as follows.

- 1) Test specimen manufacturing - Introduction of maximum fabrication defects and cosmetic repair simulation
- 2) Introduction of visible damages
- 3) Moisture pre-conditioning up to design moisture content
- 3) Limit load test in high temperature/wet condition
- 4) Two lifetime fatigue test in operational temperature/wet condition – Flight by flight load with fatigue load enhancement factor
- 5) Ultimate load test in high temperature/wet condition
- 6) Overload test in high temperature/wet condition

12.5 FULL-SCALE TESTING

12.5.1 Strength Tests for Japanese New Military Aircraft

A. Yokoyama and M. Kageyama, Third Research Center, Technical Research and Development Institute (TRDI), Japan Defense Agency, e-mail : akiz@jda-trdi.go.jp

Application of 3-D Woven Composites to Aircraft Structures

In 1989 TRDI started the preliminary research on 3-D woven composites which had fibers oriented to $0/\pm 45/90$ directions in plane and a through-the-thickness direction. Since 1994 TRDI has developed the 3-D woven composite fittings of aircraft structures: a wing root fitting, an actuator, horn fittings, and a fuselage carry-through fitting, step by step from scale components of fittings to full-scale ones shown in Figure 12.21.

Our main goals are 1) to reduce weight by 30% compared to conventional metal fittings, 2) to reinforce in a through-the-thickness direction and 3) to resist delamination by foreign object damage. Static and fatigue strength tests of the full-scale fittings are prepared.

Development of the Japanese New Maritime Patrol Helicopter (SH-60J KAI)

Since 1997 TRDI has developed the SH-60J KAI in Figure 12.22 for the Japan Maritime Self Defense Force (JMSDF). The SH-60J KAI is the modified helicopter based on the current SH-60J. The technical features in terms of the structure for the SH-60J KAI are the enlargement of the cabin and the replacement of the main rotor blades by high performance ones.

Fatigue Tests of Main Rotor Blades of the SH-60J KAI

Since 1999 bench fatigue tests have been conducted for the specimens of the main rotor blades. Figure 12.23 shows three types of the specimens: an inboard component specimen, an outboard component specimen, and a tip component specimen. The loads simulating the centrifugal force, flapping moment, edgewise bending moment, and torque are applied to each specimen. The tests are now under way.

Development of the Japanese New Search and Rescue Amphibious Aircraft (US-1A KAI)

TRDI has developed the US-1A KAI shown in Figure 12.24 for the JMSDF since 1996. The main modifications from the current US-1A in terms of the airframe structure are to pressurize the upper hull and to reduce weight of the wings, suppressor, and floats.

Full-Scale Strength Tests of the US-1A KAI

In December 2002 TRDI started the full-scale static strength tests of the US-1A KAI. More than hundred test cases which simulate flight loads, landing loads, water loads, and so forth have been conducted to certify that the US-1A KAI has enough static strength for the design loads. Figure 12.25 and Figure 12.26 show the test article and the schematic of loading frame with test article respectively. Some test cases prior to the flight have been completed successfully.

Full-Scale Fatigue Strength Tests of the US-1A KAI

The full-scale fatigue strength tests of the US-1A KAI will be started in 2003. The fatigue strength tests are composed of a durability test for two lifetimes and a damage tolerance test for two lifetimes after the durability test.

Development of the Japanese New Support Fighter (XF-2)

TRDI developed the XF-2 for the Japan Air Self Defense Force based on the USAF F-16

under the Japan-US joint-development program. The main improvements from the F-16 in terms of the aircraft structure are the enlargement of the wings, the stretch of the fuselage, and the application of advanced composites to the wings and fuselage.

12.6 AIRCRAFT ACCIDENT INVESTIGATION

12.6.1 Aircraft Accident Investigation and Aircraft Serious Incident Investigation

S. Takaoka, Aircraft and Railway Accident Investigation Commission (ARAIC),

e-mail : onoda-y2da@mlit.go.jp

(1) Total number of registration in Japan

As of December 31, 2002, the number of civil aircraft registered in Japan was 2,745 including 1,229 airplanes (of which 636 were reciprocating engine airplanes), 867 helicopters, 648 gliders including motor gliders and 1 airship.

(2) Statistics in relation to the Accident Investigation

The number of accidents that the ARAIC has investigated during past 2 years are shown in Table 12.5. The accident investigation reports were issued for 42 accidents in 2001 and 2002. The causal factors for 69% of these accidents were related to pilots, 5% to mechanical failure, 26% to weather or others.

There were 2 accidents due to mechanical failure. However these accidents were not related to fatigue failure.

(3) Statistics in relation to the Serious Incident Investigation

The serious incident means the situations which is recognized to have a risk of an accident and is determined concretely in our regulation. Before September 30, 2001, the Civil Aviation Bureau conducted the investigation of serious incidents. But, from October 1, 2001, the ARAIC has conducted serious incident investigation because of the amendment of the law. The number of serious incidents that the ARAIC investigated between October 1, 2001 and December 31, 2002 is shown in Table 12.6.

The reports were issued for 6 serious incidents. The causal factors for 2 of these incidents were related to pilots, 3 to mechanical failure, 1 to others.

Those are not related to fatigue failure.

12.7 ICAF DOUCUMENTS DISTRIBUTED BY JAPAN DURING 2001~2003

- No. 2290 On the dependence of the rate of the fatigue crack growth on the σ_a^n (2a) parameter
A. J. McEvily and S. Ishihara
- No. 2299 Experimental characterization of microscopic damage progress in AS4/PEEK cross-ply laminates under thermal cycling
K. Terada, S. Kobayashi and N. Takeda
- No. 2300 Experimental and analytical characterization of matrix cracking in quasi-isotropic CFRP laminates with interlaminar-toughened layers under fatigue loading
S. Kobayashi, S. Ogihara and N. Takeda
- No. 2301 Experimental characterization of matrix cracking behavior in thermally cycled CFRP laminates
S. Ogihara, A. Kobayashi, T. Ishiguro and N. Otani
- No. 2302 Effect of thermal cycling on microcracking and strength degradation of high-temperature polymer composite materials for use in next-generation SST structures
T. Shimokawa, H. Kato, Y. Hamaguchi, S. Sanbongi, H. Mizuno, H. Nakamura, R. Asagumo and H. Tamura
- No. 2303 Effects of stress waveform and water absorption on the fatigue strength of angle-ply aramid fiber/epoxy composites
K. Komai, K. Minoshima, K. Tanaka and T. Tokura
- No. 2304 Thermal fatigue failure induced by delamination in thermal barrier coating
Y. C. Zhou and T. Hashida
- No. 2305 Two-stress level fatigue of unidirectional fiber-metal hybrid composite : GLARE 2
M. Kawai and A. Hachinohe
- No. 2306 Effects of loading frequency and environment on delamination fatigue crack growth of CFRP
Y. Nakai and C. Hiwa
- No. 2307 Mode I and II delamination fatigue crack growth behavior of alumina fiber / epoxy laminates in liquid nitrogen
M. Hojo, S. Matsuda, B. Fiedler, T. Kawada, K. Moriya, S. Ochiai and H. Aoyama
- No. 2308 Structural fatigue and joint degradation
H. Terada

ACKNOWLEDGMENTS

Dr. Shinji Ogihara, Associate Professor of Tokyo University of Science, is greatly appreciated for his elaborate preparation during the course of compilation of present national review.

Table 12.1 Demonstration Themes

| # | Demonstration Categories | Demonstration Themes |
|---|--------------------------------------|---|
| 1 | Real Time Detection of Impact Damage | Optical Fiber Sensors Embedded into CFRP Laminated Structures |
| 2 | | Integrated Acoustic Emission Sensor Network Systems |
| 3 | Damage Detection | Strain Distribution Measurement in Wide Area Using Distributed BOTDR Sensors |
| 4 | | Damage Detection by Electric Conductivity Change in Smart Patch (Carbon Fiber Composite Sheets) |
| 5 | Damage Suppression | Damage Suppression System Using Embedded SMA (Shape Memory Alloy) Foils |
| 6 | Smart Manufacturing | Smart Manufacturing of Low Cost Integrated Panel by RTM (Resin Transfer Molding) |
| 7 | Noise and Vibration Reduction | Noise and Vibration Reduction Technology in Aircraft Internal Cabin |

Table.12.2 Stacking sequence of coupon test specimens

| No. | Stacking Sequence | Test temp |
|-----|---|-----------|
| 1 | [45/0/-45/90]s | RT |
| 2 | [45/0/-45/90]s | 80°C |
| 3 | [45/0/-45/Ad/0% Pre-strained SMA/Ad/90]s | RT |
| 4 | [45/0/-45/Ad/0% Pre-strained SMA/Ad/90]s | 80°C |
| 5 | [45/0/-45/90/Ad/2% Pre-strained SMA/Ad/90/-45/0/45] | RT |
| 6 | [45/0/-45/90/Ad/2% Pre-strained SMA/Ad/90/-45/0/45] | 80°C |

Table.12.3 Damage onset strain of coupon test specimen

| T/P No. | Type of Specimen | Transverse Crack (%) | Delamination (%) |
|---------|-------------------------------|----------------------|------------------|
| 1 | CFPR Only RT | 0.67 | 0.77 |
| 2 | CFPR Only RT | 0.65 | 0.83 |
| 3 | CFPR/0% Pre-Strained SMA RT | 0.7 | 1.0 |
| 4 | CFPR/0% Pre-Strained SMA 80°C | 0.75 | over 1.3 |
| 5 | CFPR/2% Pre-Strained SMA RT | 0.84 | 1.1 |
| 6 | CFPR/2% Pre-Strained SMA 80°C | 0.89 | over 1.3 |

Table.12.4 Condition of fatigue test

| Stress Ratio | Test Strain | Condition | Frequency |
|--------------|-------------|--------------------------|-----------|
| 0.1 | 0.30% | R.T. DRY or 80°C, DRY | 10Hz |
| | 0.40% | | |
| | 0.50% | | |
| | 0.60% | | |

Table 12.5 Number of Accidents investigated in Japan for past 2 years

| Aircraft type | Airplane | Helicopter | Glider and Motor glider | Others (ULP etc.) | Total |
|---------------|----------|------------|----------------------------|----------------------|--|
| 2001 | 8✕ | 8✕ | 4 | 2 | 22✕ including 1 mid-air collision |
| 2002 | 8 | 15 | 7 | 5 | 35 |

Table 12.6 Number of Serious incidents investigated in Japan between Oct.1, 2001 and Dec. 31, 2002

| Aircraft type | Airplane | Helicopter | Glider and Motor glider | Others (ULP etc.) | Total |
|---------------|----------|------------|----------------------------|----------------------|-------|
| 2001 | 3 | 0 | 0 | 0 | 3 |
| 2002 | 1 | 1 | 1 | 2 | 5 |

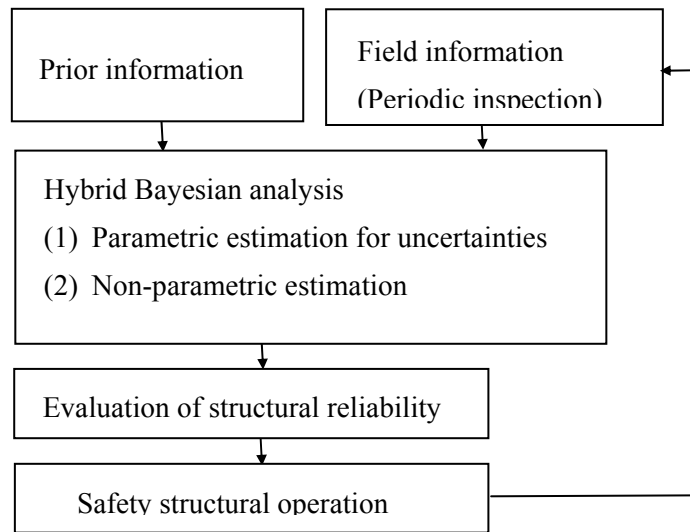


Figure 12.1 Concept of HYBAC analysis

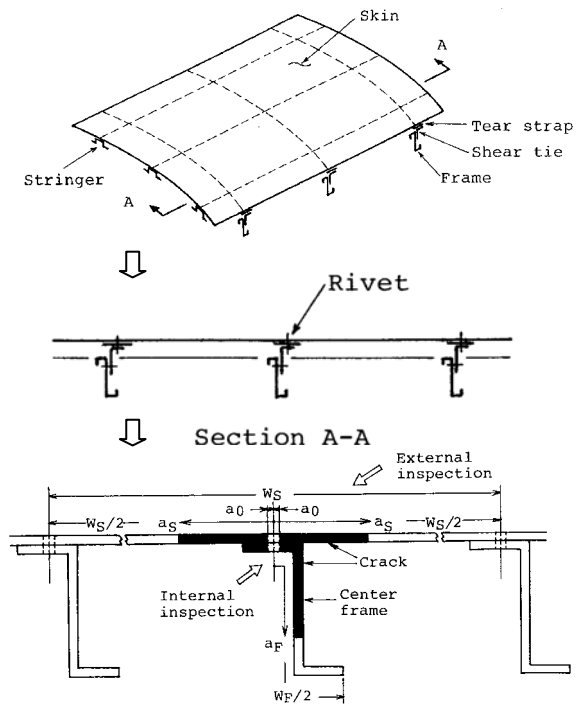


Figure 12.2 Fatigue critical element of fuselage structure

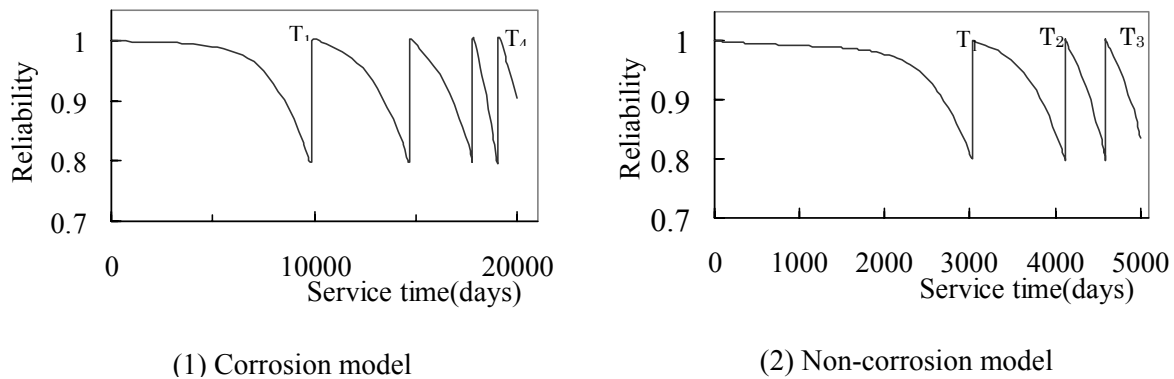


Figure 12.3 Inspection schedule and structural reliability

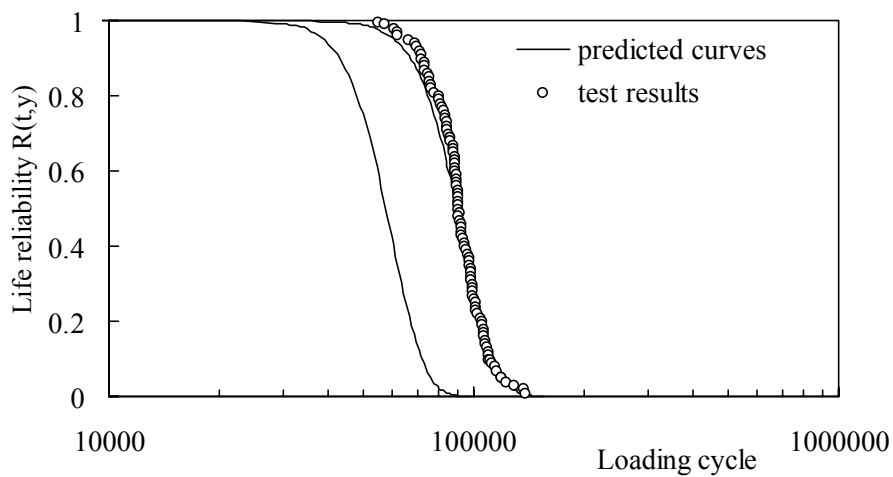


Figure 12.4 LY12CZ specimens life reliability curves(left/right curves: with/without effect of corrosion and ageing)

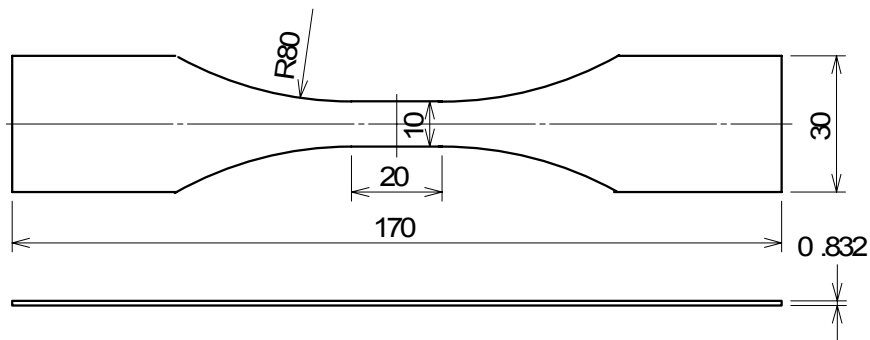


Figure 12.5 Specimen shape.

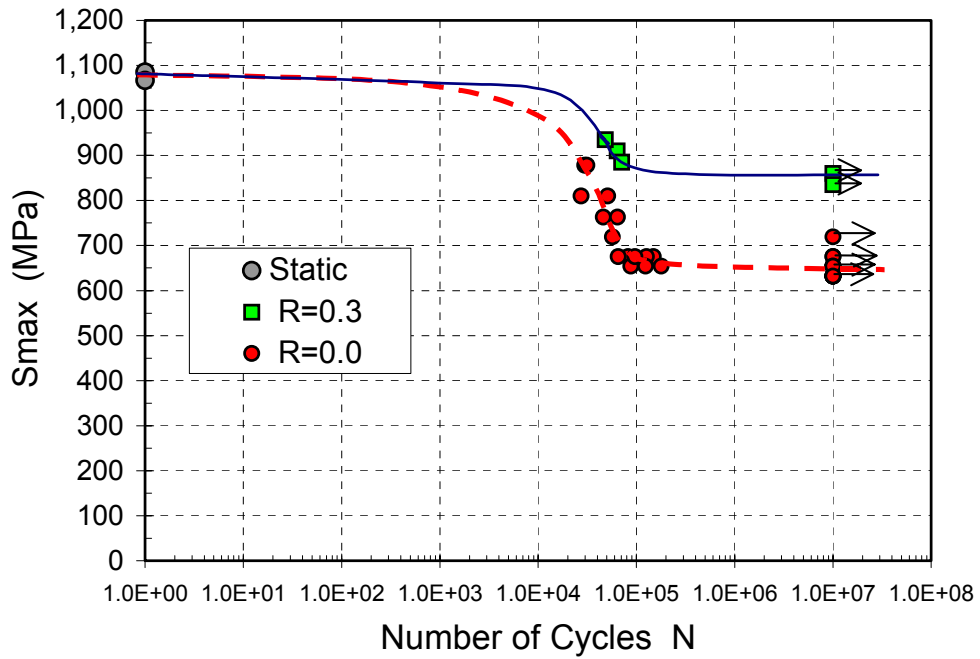


Figure 12.6 S - N relationships, represented by S_{max} .

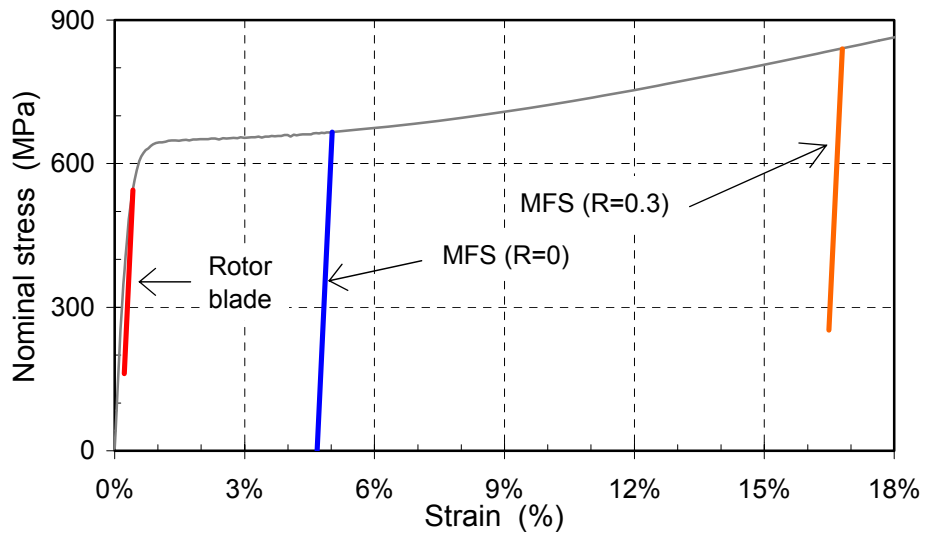


Figure 12.7 Comparison of the design strain range with the mean fatigue strength (MFS) at 10^7 cycles for $R=0$ and 0.3.



Figure 12.8 MHI-1 Door assembly



Figure 12.9 MHI-2 Test specimen

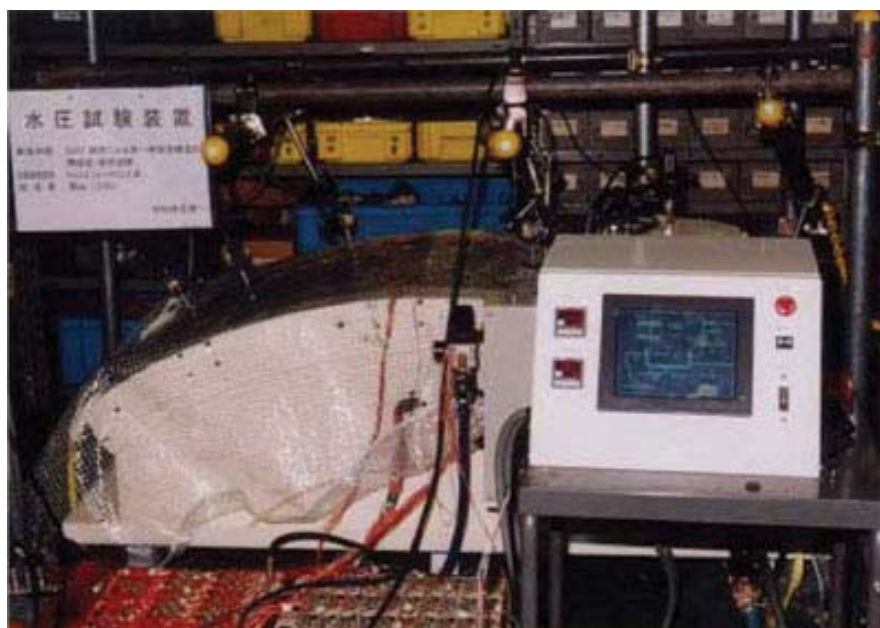


Figure 12.10 MHI-3 Test set-up

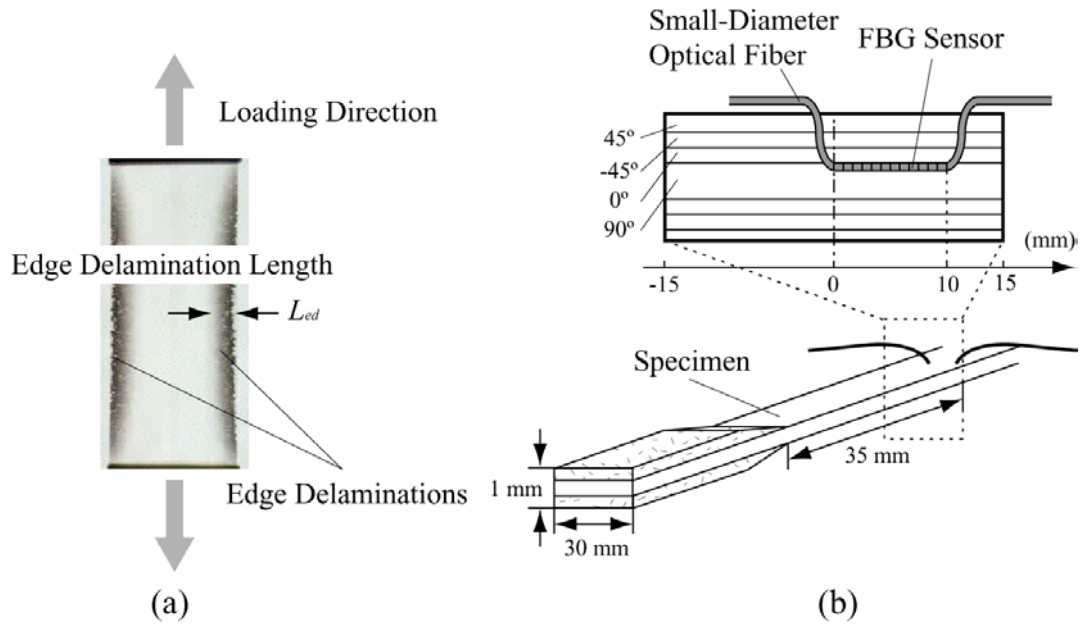


Figure 12.11 A soft X-ray photograph of the delaminated specimen (a) and illustration of specimen with an embedded small-diameter FBG sensor (b).

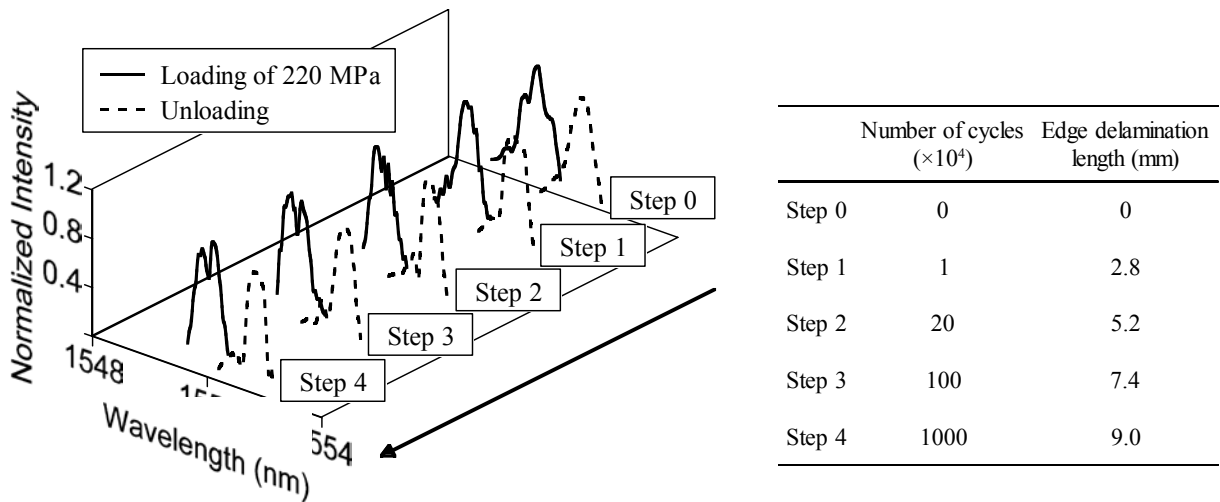


Figure 12.12 Measured reflection spectra for different numbers of cycles and edge delamination length, L_{ed} .

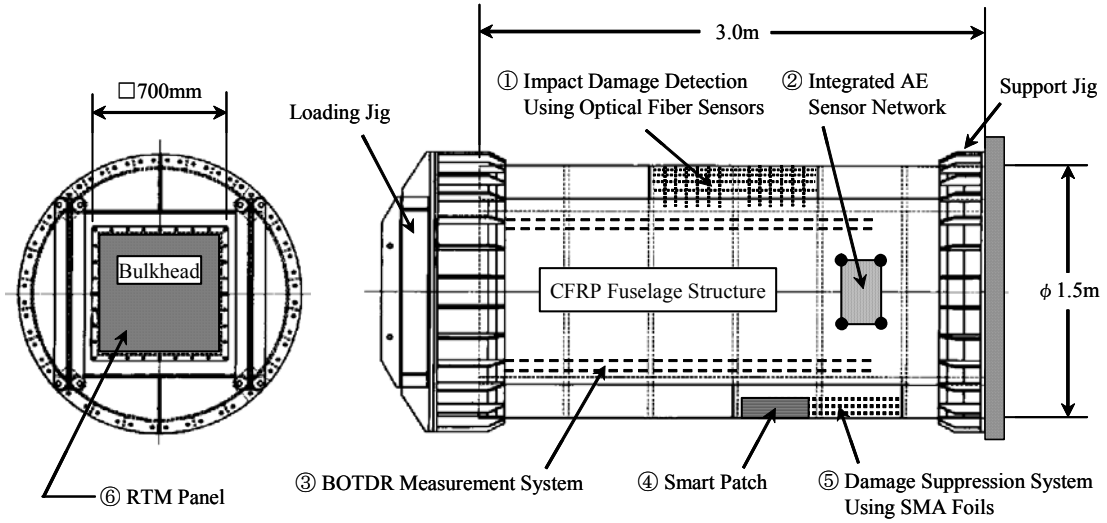


Figure 12.13 Outline of the damage detection and suppression demonstrator

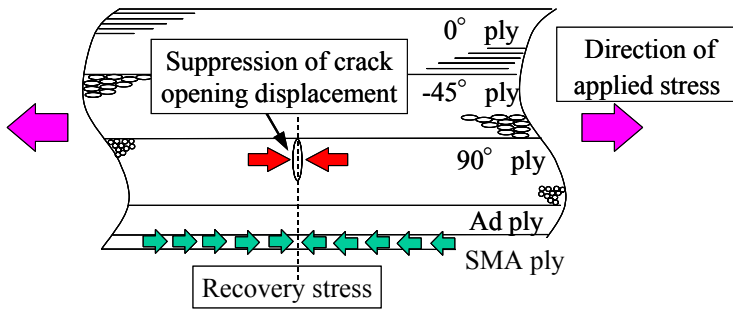


Figure.12.14 Concept of damage suppression effects



Figure.12.15 Setup of load-unload test

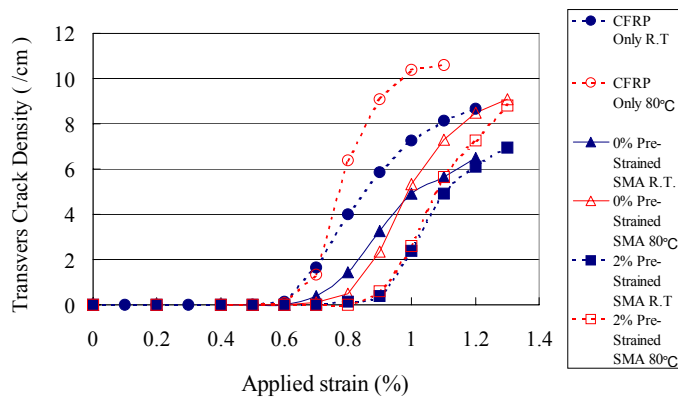


Figure.12.16 Transverse crack density as a function of applied strain on some kinds of CFRP laminates with and without embedded SMA foils

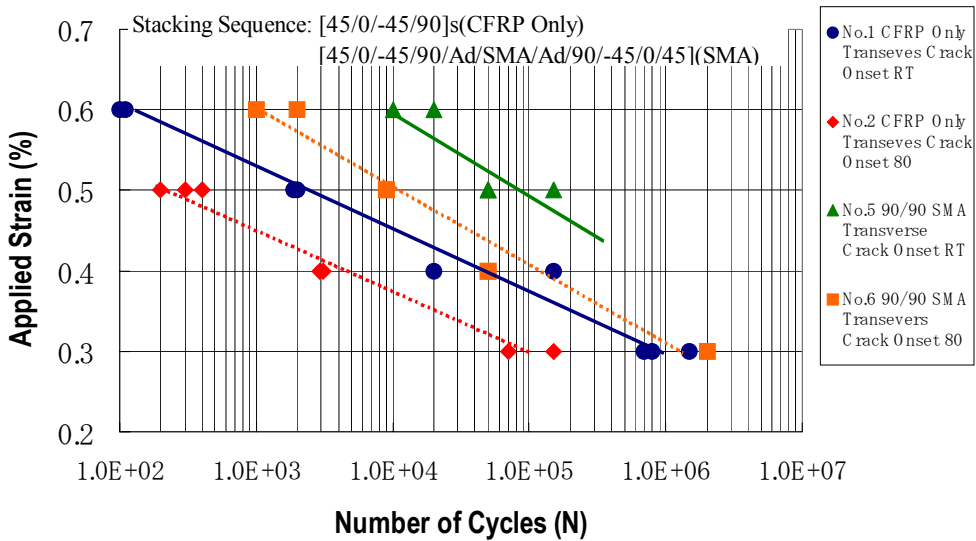


Figure.12.17 Comparison on number of cycles for onset of transverse crack on CFRP laminates with and without embedded SMA foils in the center of the laminates

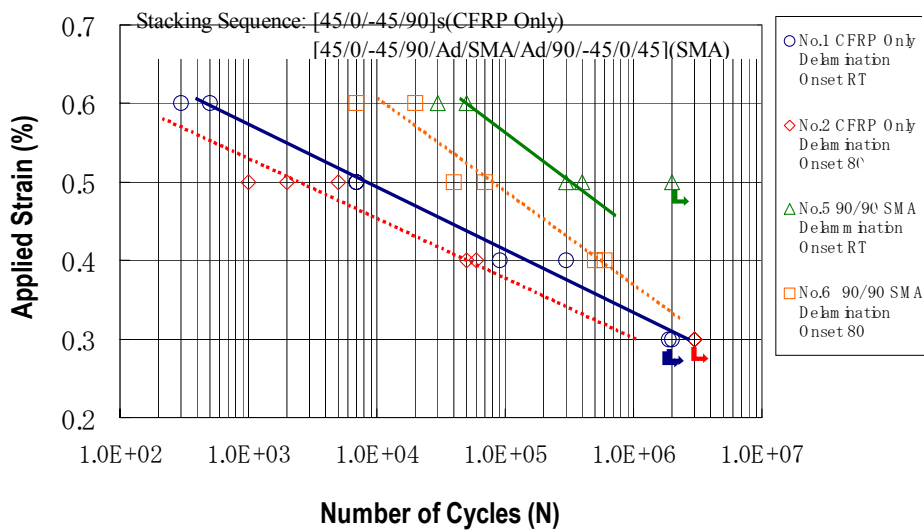


Figure.12.18 Comparison on number of cycles for onset of delamination on CFRP laminates with and without embedded SMA foils in the center of the laminates.

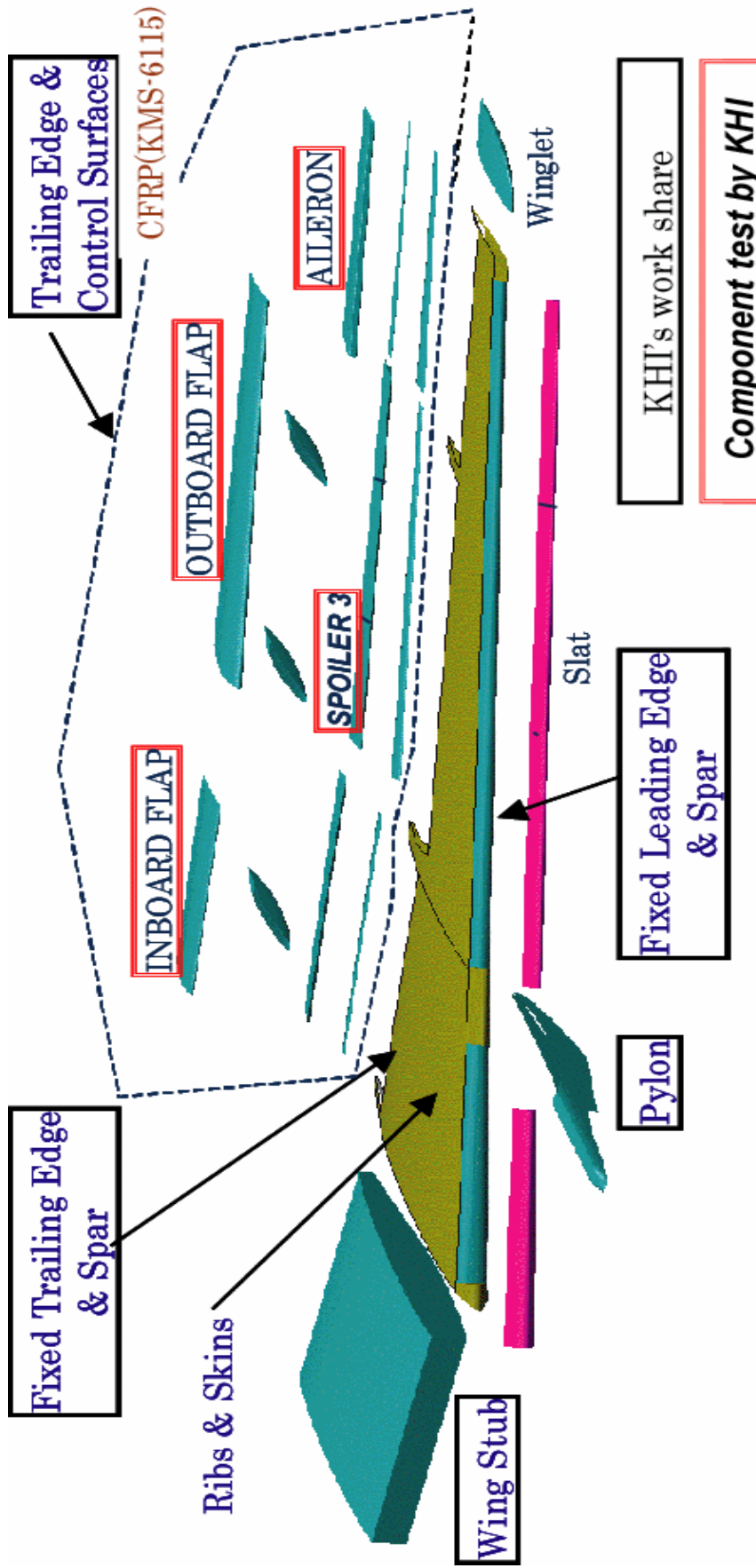


Figure 12.19 Work share and component test items



Inboard Flap - set up



Aileron -set up



Inboard Flap -set up



Outboard Flap - specimen



Spoiler - specimen

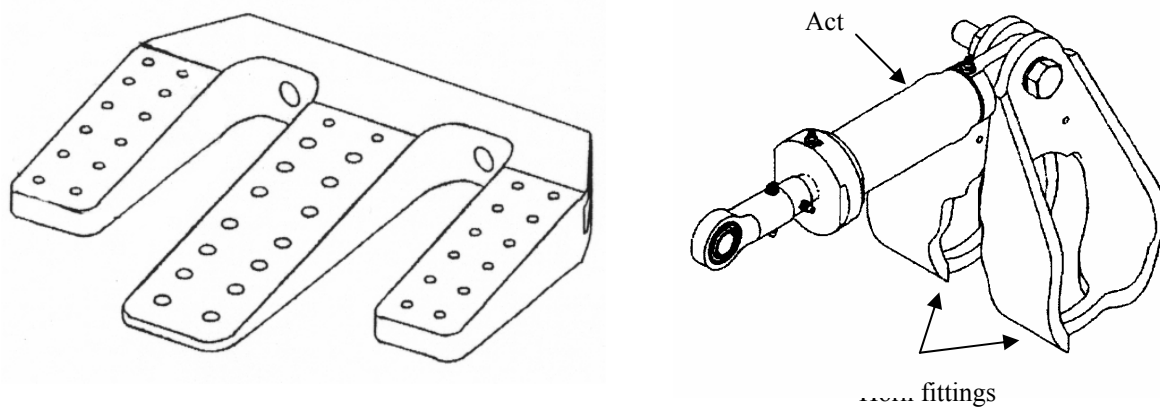


Outboard Flap - set up

< Structural Strength Test >

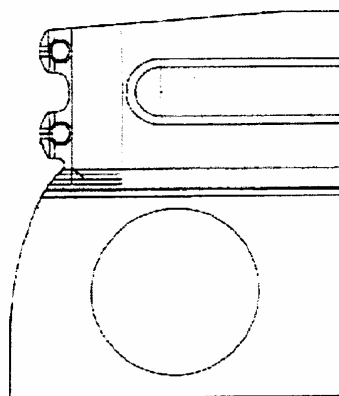
< Mechanism Operation Test >

Figure 12.20 Photographs of full scale component tests of wing control surfaces



(1) Wing root fitting

(2) Actuator and horn fittings



(3) Fuselage carry-through fitting

Figure 12.21 3-D woven composite fittings



Figure 12.22 Japanese new maritime patrol helicopter (SH-60J KAI)

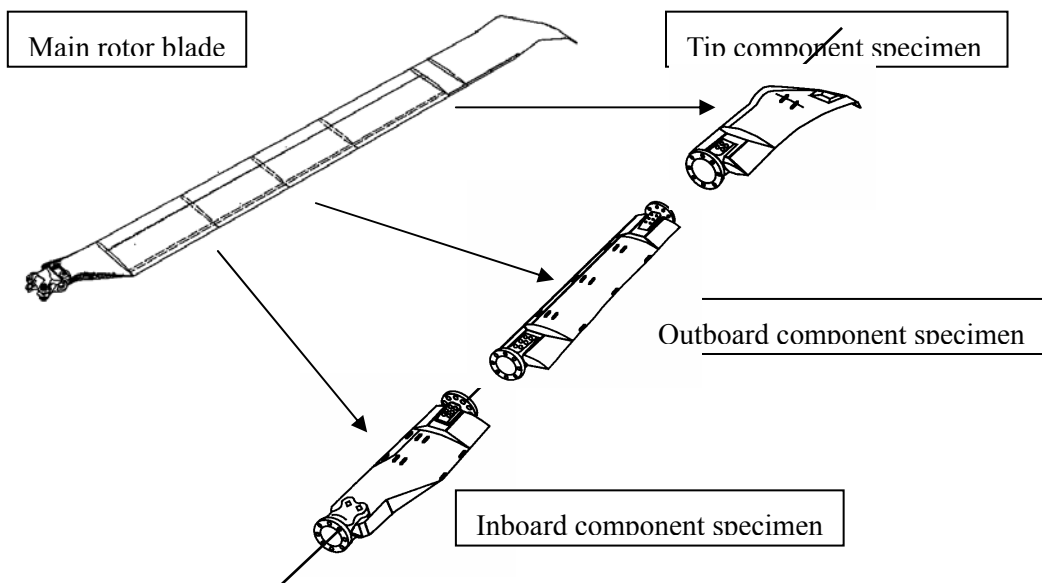


Figure 12.23 Test specimens for fatigue tests of main rotor blade



Figure 12.24 Japanese new search and rescue amphibious aircraft (US-1A KAI)

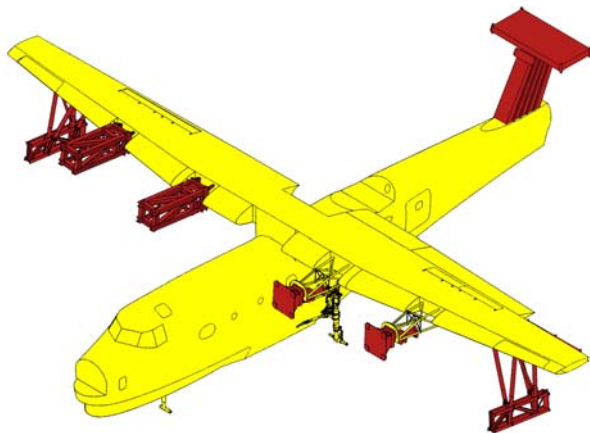


Figure 12.25 Static strength test article

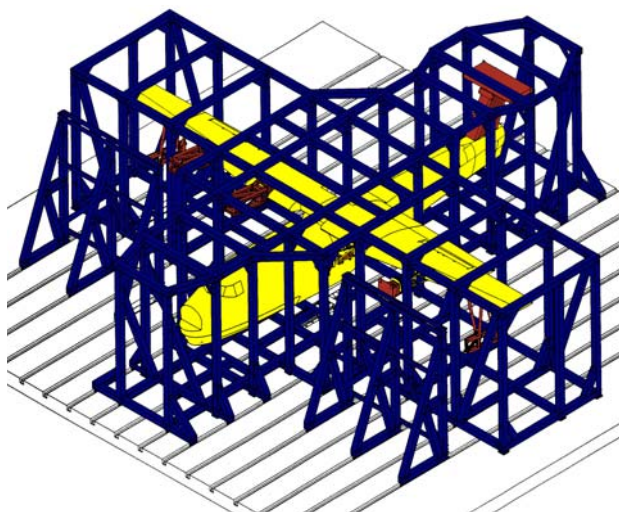


Figure 12.26 Schematic of loading frame